Effect of phosphorous content on the microstructure and erosion–corrosion resistance of electrodeposited Ni-Co-Fe-P coatings

Xiulin Ji [a,b,*], Chunyan Yan [b], Hui Duan [a], Chanyuan Luo [a]

[a] Engineering Research Center of Dredging Technology of Ministry of Education, Hohai University, Changzhou 213022, China
[b] College of Mechanical & Electrical Engineering, Hohai University, Changzhou 213022, China

ABSTRACT

Ni-Co-Fe-P quaternary alloy coatings were electrodeposited and the dependence of microstructure and erosion–corrosion resistance with varying P content was investigated. With the addition of H_3PO_3 from 0 to 40 g L^{-1} into the electrolyte bath, the P content in Ni-Co-Fe-P quaternary alloy coating increased to 12.92 wt%. Along with the increase of P content, the microstructure evolved from a composite structure of crystalline and amorphous to a pure amorphous and then to another composite structure, while the grain size refined gradually and the microhardness increased obviously from about 510 to 1150 HV. The corrosion rate and the synergy between erosion and corrosion first increased and then decreased with the increase of P content. The polarization curves detected in the slurry flow at impact velocity of 4.19 m s^{-1} shows a tendency to passivity for all of as-deposited coatings. Ni-Co-Fe-12.92P coating deposited from H_3PO_3 concentration of 40 g L^{-1} possesses the best erosion–corrosion resistance due to the highest hardness and the lowest corrosion current density. Large amounts of cracking lips along the micro-plowing grooves can be observed on the worn surface morphologies of as-deposited coatings and the predominant wear mechanism is mechanical micro-cutting in Ni-Co-Fe-P coatings when subjected to erosion–corrosion in slurry flow.

© 2016 Elsevier B.V. All rights reserved.

1. Introduction

Erosion–corrosion is a common degradation of those materials applied in the two-phase fluid, especially oil-sand or saline-sand slurry [1–2]. In order to improve the erosion resistance of fiber reinforced plastics, electrodeposited protective metallic layers have been considered [3]. And the electrolytic deposition of a Ni-Co based coating on carbon steel is capable of enhancing significantly the hardness and resistance to wear and corrosion of the steel in oil-sand slurry [1]. Our previous work also showed a possible way to improve the erosion–corrosion resistance of steel by electrodeposited coatings [4].

Based on the nickel electroplating, co-deposition of cobalt with nickel was studied extensively for the improvement of mechanical properties and corrosion resistance [5]. In recent years, the triple Ni-Co-Fe alloys have been intensively studied because these ternary alloys show higher saturation induction and lower coercive field than the binary magnetic alloys [6]. Actually, Ni-Co-Fe alloy coating is also attracting as an important transition metal alloy for its outstanding

physical and chemical properties [7]. Its hardness, corrosion resistance and superficial radiance are close to that of the hard chromium deposit and may replace the actual widely used hard chromium plating in certain degree [8].

Since it has been acknowledged that the hardness, wear and corrosion resistance of Ni-P coatings are obviously influenced by phosphorous incorporation [9–10], various P contents were investigated in order to understand the effect of the composition on mechanical properties of Ni-P electrodeposits [11]. Accordingly, the microstructure of amorphous, nanocrystalline and their composites were obtained with different phosphorous contents [9–11]. Moreover, the addition of 0.45 M sodium hypophosphite to the chloride base electrolyte also can improve the corrosion resistance of electrodeposited coatings [12]. Therefore, phosphorous addition was supposed to improve the hardness, wear and corrosion resistance of Ni-Co-Fe coatings. However, the literatures on Ni-Co-Fe-P quaternary alloy coatings were very limited. With adding H_3PO_3 into the electrolyte bath, Ni-Co-Fe-P coating was electrodeposited and it has higher hardness, lower friction coefficient and wear rate compared to the electrodeposited Ni-Co-Fe ternary alloy coating [13]. However, it is still not clear about the influence of phosphorous contents on the physical or chemical properties. Thus, in this work, the dependence of microstructure and erosion–corrosion

---

* Corresponding author at: Engineering Research Center of Dredging Technology of Ministry of Education, Hohai University, Changzhou 213022, China.
E-mail address: xiulinji@gmail.com (X. Ji).

resistance on various phosphorous contents of electrodeposited Ni-Co-Fe-P coatings has been investigated.

2. Experimental work

2.1. Electrodeposition of Ni-Co-Fe-P alloy coatings

Ni-Co-Fe-P alloy coatings with about 30 ~ 40 μm thickness were electrodeposited galvanostatically from the electrolyte consisting of $NiSO_4 \cdot 6H_2O$ 120 g L^{-1}, $NiCl_2 \cdot 6H_2O$ 40 g L^{-1}, $FeSO_4 \cdot 7H_2O$ 20 g L^{-1}, $CoCl_2 \cdot 7H_2O$ 10 g L^{-1} and other additives. During electrodeposition, H_3PO_3 concentration (10 ~ 40 g L^{-1}) was adjusted to produce Ni-Co-Fe-P alloy coatings with various P contents. All chemicals were reagent grade and dissolved in distilled water. The pH value of the solution was adjusted to 1.8. A pure nickel sheet and a cylindrical AISI 1045 steel rod with 4 mm diameter and 40 mm long were used as anode and cathode respectively. A current density of 2 A dm^{-2} and temperature of 65 °C were maintained throughout the plating runs. And the plating time was controlled in 3 h. After electrodeposition, samples were rinsed in running water and ethanol, dried in hot air, and then preserved for characterization and erosion–corrosion test.

2.2. Material characterization

The coatings were characterized by X-ray diffraction (XRD) analysis to determine the structure. The surface morphology and chemical composition were obtained by S3400 scanning electron microscope (SEM) equipped with energy dispersive spectroscopy (EDS). The microhardness was detected using HXD-1000TC digital microhardness tester by GB4342-84 standard and measured at out of 5 randomly located positions on the electrodeposited surface for each sample. A constant load of 0.98 N was applied for 15 s to cause the indentations in the deposits. An average of five readings was taken as hardness value for each sample. Electrochemical measurements were carried out by PS-268A system (Beijing, China) with a platinum counter electrode and a saturated calomel electrode (SCE) reference electrode in 3.5% NaCl aqueous solution for static corrosion and in sand containing slurry for dynamic corrosion. Prior to electrochemical tests, the samples were kept in 3.5 wt% NaCl solution at room temperature and Open Circuit Potential (OCP) was measured and recorded until no further changes were observed (<10 mV h^{-1}). All corrosion tests were carried out in a standard three-electrode cell, where the electrodeposited steel rod was used as working electrode (WE), a saturated calomel electrode (SCE) as reference electrode and a platinum plate as auxiliary electrode. At least two tests were performed for each sample in order to confirm reproducibility of the results.

2.3. Erosion–corrosion test

The erosion–corrosion tests were conducted by a slurry pot erosion tester (MSH type erosion–corrosion system, China) equipped with electrochemical detective system. It is mainly consisted of a rotating device and the schematic diagram of the erosion tester was shown in Fig. 1, which was also described by Rajahram et al. [14]. The samples were mounted on the holder at the edge of the rotating disk with 20 mm diameter and the motor drove the sample rotary in the slurry at the rotation velocity of 400 rpm. The impact velocity means the particle's velocity as impacting the sample and it can be looked as the velocity difference between the rotation and the flow. So the real impact velocity is lower than the rotation velocity. Because the rotation velocity is easy to detect and useful for comparing erosion–corrosion with impact velocity, the line speed of the rotation disk was used to represent the impact velocity (V_i). It can be calculated from the diameter (D) and the rotation velocity (V_r) using this equation $V_i = \pi D V_r$. So the nominal impact velocity is 4.19 m s^{-1} at the rotation velocity of 400 rpm in this study. Silica sands with mean size of 250 ~ 550 μm were used in our erosion–

corrosion tests. Each erosion–corrosion test was performed for 3 h and the slurry pot was filled with 10 L aqueous solution containing 10 wt% sand particles and 3.5% NaCl. The old slurry was replaced by fresh one for every three tests. In this present study, the mass loss caused by pure erosion (W_e) was assumed to be equal to mass loss in distilled water containing 10 wt% sand particles without NaCl addition. To the mass loss caused by pure corrosion (W_c), test was carried out in 3.5% NaCl solution without sand particles. The synergism between erosion and corrosion (W_s) was expressed as the difference between the total mass loss (W_t) and the sum of W_e and W_c. Three replicate wear tests were carried out so as to minimize data scattering. All the samples were firstly ground by SiC paper in a grit of #800 and degreased in acetone, then cleaned in an ultrasonic bath by ethanol and air-dried in desiccators before gravimetric mass loss measurements were made. Gravimetric measurements were performed using a precision balance with an accuracy of ± 0.1 mg. Measurements were repeated six times for each sample and the maximum and minimum values were discarded. The remaining 4 readings were averaged to obtain an average mass loss for each test sample. All electrochemical measurements and erosion–corrosion tests were conducted at ambient temperature.

3. Results and discussion

3.1. Morphology and chemical composition

Fig. 2 depicts the surface morphologies of Ni-Co-Fe-P alloy electrodeposits with different P contents. A colony-like morphology having various sizes is seen in all of the samples. And each colony could be found to contain several smaller grains. Similar surface morphologies of as-deposited coating were also observed in Ni-Co-W [15] and Ni-P [16] alloys. It is noticeable that the cracks on Ni-Co-Fe-P alloy deposited from the electrolyte containing 10 g L^{-1} H_3PO_3, which suggesting a high internal stress was generated in the coating deposited at this H_3PO_3 concentration. With the increase of H_3PO_3 concentration, smaller colony-like structure is obtained. This indicates phosphorous incorporation is beneficial to grain size refinement of Ni-Co-Fe-P alloy coatings.

The typical EDS patterns of Ni-Co-Fe-P alloy coatings deposited from various H_3PO_3 concentrations are displayed in Fig. 3. And the corresponding data obtained from EDS are listed in Table 1. As it can be seen, the P content in Ni-Co-Fe-P coating increases with the increase of H_3PO_3 concentration in the plating bath. With the increasing of H_3PO_3 concentration from 10 to 40 g L^{-1}, P content increased from 5.60 to 12.92 wt%. Moreover, not only the contents of other elements consisting of Ni-Co-Fe-P alloy decreased but also their relative content percentages varied with the increase of H_3PO_3 concentration.
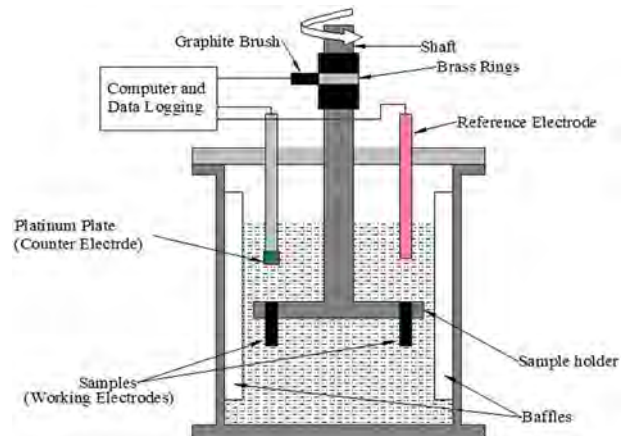

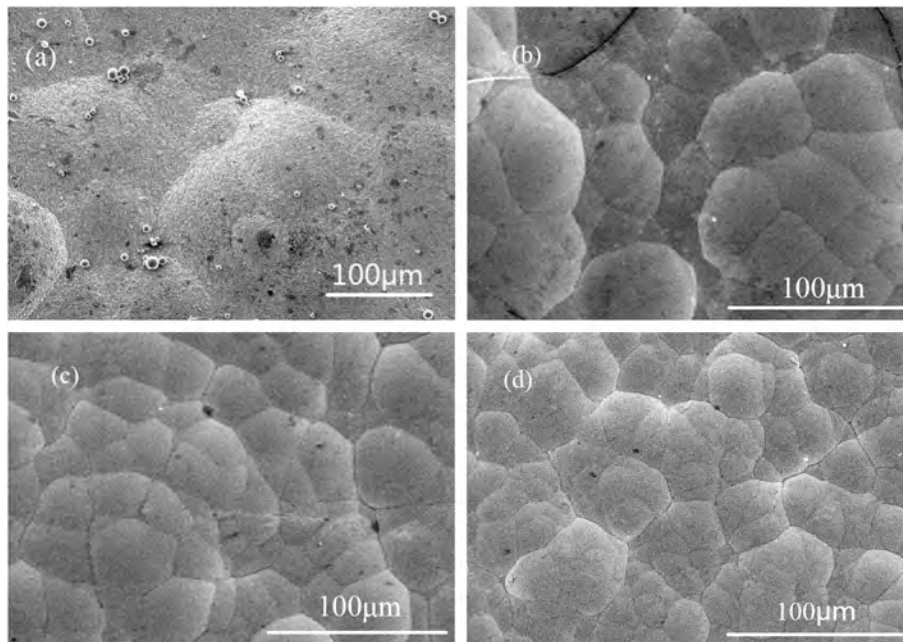**Fig. 1.** Schematic diagram of MSH type erosion–corrosion tester.

Fig. 2. SEM images of Ni-Co-Fe-P coatings deposited from different H_3PO_3 concentration (a) 0 g L^{-1}, (b) 10 g L^{-1}, (c) 20 g L^{-1} and (d) 40 g L^{-1}.

3.2. Microstructure and hardness

The XRD patterns of the electrodeposited Ni-Co-Fe-P coatings obtained from different H_3PO_3 concentrations are shown in Fig. 4. A sharp diffraction peak resulting from (200) of Ni was observed for the Ni-Co-Fe coating without other phase for the very low content of Co and Fe, as shown in Table 1. A composite structure with Ni_3P, $FeNi_3$, Ni

and amorphous phase can be deduced for Ni-Co-Fe-P coating deposited from 10 g L^{-1} H_3PO_3 concentration. The (200) intensity markedly decreases while the (111) intensity increases for the Ni-Co-Fe-5.6P coating, indicating that P tends to retard the growth rate of (111) facets as compared to that of (200) [10]. With the H_3PO_3 concentration increasing to 20 g L^{-1}, the as-deposited Ni-Co-Fe-P coating shows a broad diffraction halo, implying the formation of amorphous microstructure. As
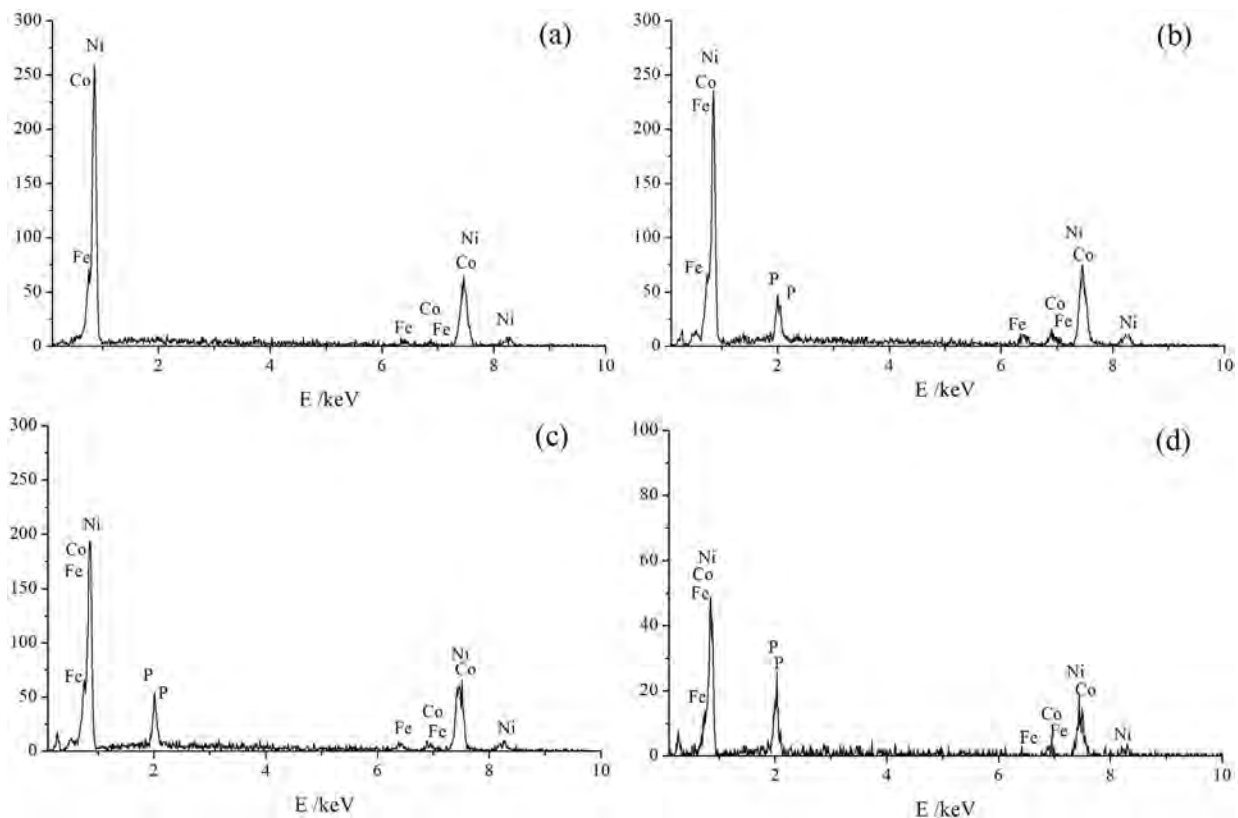

Fig. 3. EDS patterns of Ni-Co-Fe-P alloy coatings fabricated from different H_3PO_3 concentration: (a) 0 g L^{-1}, (b) 10 g L^{-1}, (c) 20 g L^{-1} and (d) 40 g L^{-1}.

Table 1
Compositions of Ni-Co-Fe-P coatings as a function of H_3PO_3 concentration.

H_3PO_3 concentration (g L^{-1})	Fe (wt%)	Co (wt%)	Ni (wt%)	P (wt%)
0	1.47	2.58	94.92	0
10	4.82	8.69	80.89	5.60
20	3.81	5.60	82.66	7.93
40	1.92	11.14	74.02	12.92

the P content was further increased by H_3PO_3 concentration increasing to 40 g L^{-1}, an amorphous structure mixed with Fe_7Ni_3, $CoFe_7$ or $Fe_{19}Ni$ was observed. Due to the electronegativity difference, Ni, Co and Fe have strong chemical affinity with P. Moreover, because of atomic size difference, the alloying of P causes a distortion of the base Ni-Co-Fe solid solution lattices during the electrodeposition. And the greater the P deposition results in the greater the degree of disorder, and the greater the percentage of amorphous phase. When P deposition is further increased to near eutectic composition, the structure of coating is amorphous [9]. As further increasing P content higher than eutectic composition, the structure of coating is in an amorphous and nanocrystalline mixed microstructure.

Fig. 5 presents the microhardness profiles measured on the cross-sectional plane perpendicular to the surface coated with Ni-Co-Fe-P alloys under different H_3PO_3 concentration. The region of high hardness corresponding to coating thickness is confined up to about 40 μm depth from the surface. The microhardness of the Ni-Co-Fe-P alloy increased from about 510 to 690 HV when the H_3PO_3 concentration increased from 0 to 10 g L^{-1}. As the H_3PO_3 concentration further increased to 20 g L^{-1}, the highest microhardness (about 1150 HV) of Ni-Co-Fe-P alloy can be obtained. However, when the H_3PO_3 concentration increased to 40 g L^{-1} H_3PO_3 concentration, the microhardness does not improved obviously but keeps above 1100 HV. Therefore, because of P incorporation, the microhardness of Ni-Co-Fe-P alloy is significantly improved as compared to the Ni-Co-Fe alloy.

3.3. Corrosion resistance

In order to quantitatively analyze the corrosion resistant, anodic polarizations of Ni-Co-Fe-P and Ni-Co-Fe alloy coatings in 3.5 wt% NaCl solution were employed, as shown in Fig. 6. The corresponding corrosion potential (E_{corr}) and corrosion current density (i_{corr}) of test materials were estimated from the polarization curves by the Tafel extrapolation method and listed in Table 2. The i_{corr} of Ni-Co-Fe-P coating increased obviously from 0.92 to 9.23 μA cm^{-2} with addition of 10 g L^{-1} H_3PO_3.
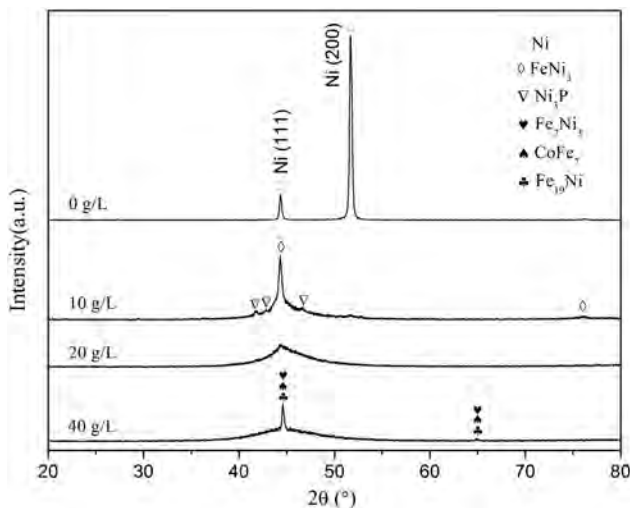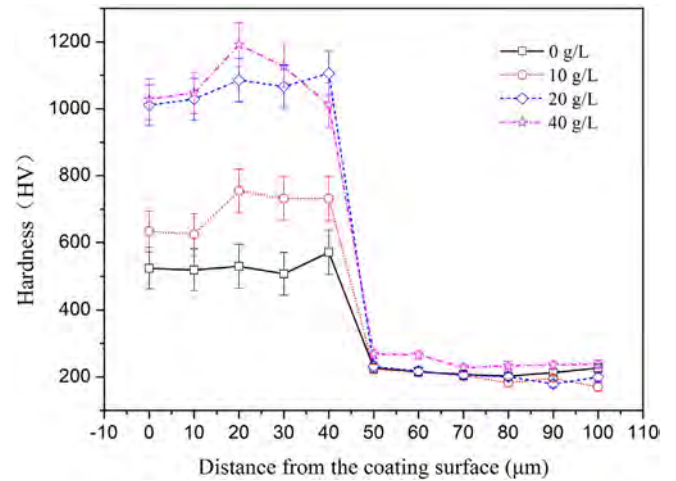
Fig. 5. Cross-section microhardness profiles of Ni-Co-Fe-P coatings as a function of distance from the coating surfaces.

It suggests that the multiphase (Ni_3P, $FeNi_3$, Ni and amorphous phase) structure caused by P alloying destroys the microstructure uniform of single phase, thus reducing the corrosion resistance. With the further increasing H_3PO_3 concentration from 20 to 40 g L^{-1}, i_{corr} continually decreased to 0.11 μA cm^{-2}. It indicates the microstructure homogenization (as shown in Fig. 4) and grain size refinement (as shown in Fig. 2) are beneficial to reduce corrosion rate. As seen from Fig. 6, the passive film formation is possible for the Ni-Co-Fe-P coatings. It is accepted that the passive film formation on the corroded surface of metals is a diffusion controlled process while the diffusion rate of elements in nanocrystalline metals would be as high as to facilitate the formation of passive films [16]. In this case, lower corrosion rate is expected to be obtained for the coating with smaller grain size and more uniform microstructure. So the Ni-Co-Fe-P coating with near-eutectic composition leads to the formation of dense passive films and thus very low corrosion rate.

To show the influence of impact velocity on corrosion resistance, the typical polarization curves for Ni-Co-Fe-P alloy coatings with different P content in 3.5% NaCl solution containing 10 wt% sand particles at impact velocity of 4.19 m s^{-1} are illustrated in Fig. 7 and the corresponding E_{corr} and i_{corr} are summarized in Table 3. For 4.19 m s^{-1} impact velocity, the free corrosion potentials of all the Ni-Co-Fe-P coatings shift toward positive direction and their polarization curves exhibit a tendency to passivity. As shown in Table 2, comparing with the static state, the i_{corr} of
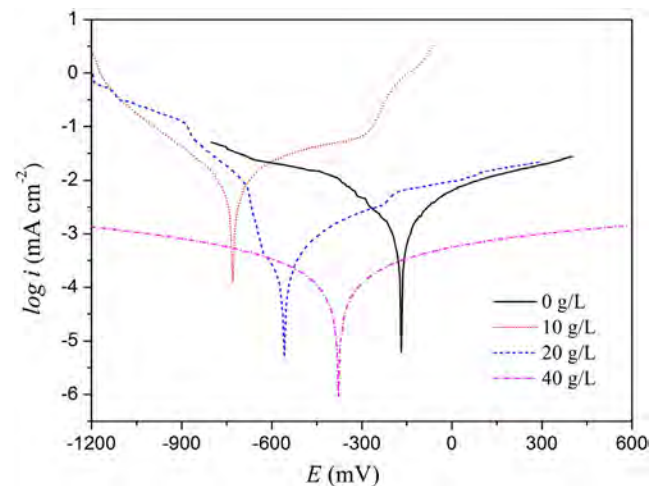
Fig. 4. XRD patterns of Ni-Co-Fe-P alloy coatings electrodeposited from different H_3PO_3 concentration.

Fig. 6. Potentiodynamic polarization curves of Ni-Co-Fe-P alloy coatings as a function of H_3PO_3 concentration in 3.5% NaCl solution.

Table 2
Corrosion potential (E_{corr}) and corrosion current density (i_{corr}) of Ni-Co-Fe-P alloy coatings under 3.5% NaCl solution containing 10 wt% sand particles.

H_3PO_3 concentration (g L^{-1})	E_{corr} (mV)	i_{corr} (μA cm^{-2})
0	−168	0.92
10	−728	9.23
20	−558	0.21
40	−378	0.11

Table 3
Corrosion potential (E_{corr}) and corrosion current density (i_{corr}) of Ni-Co-Fe-P alloy coatings under 3.5% NaCl solution containing 10 wt% sand particles at impact velocity of 4.19 m s^{-1}.

H_3PO_3 concentration (g L^{-1})	E_{corr} (mV)	i_{corr} (μA cm^{-2})
0	567	0.22
10	522	0.43
20	632	0.21
40	667	0.18

Ni-Co-Fe-5.6P coating at impact velocity of 4.19 m s^{-1} is much lower. However, Ni-Co-Fe-12.92P coating still possesses the best corrosion resistance. Because of the increasing of E_{corr} and decreasing of i_{corr}, it suggests a passive film could be formed on the surface of Ni-Co-Fe-P coating. It is different with the general trends are for a decrease in corrosion potential and an increase in corrosion current density with increasing impact velocity [17]. Actually, a passive film has an ability to inhibit corrosion as long as erosion–corrosion [18] and it is potential to improve the erosion–corrosion resistance of Ni-Co-Fe-P coatings.

3.4. Erosion–corrosion resistance

The combined effects of erosion and corrosion can be significantly higher than the sum of the effects of them separately. This net effect is called synergism and it is related to the material's corrosion resistance as well as its erosion resistance [19–20]. The total mass loss in slurry flow can be expressed as follows,

$$W_t = W_e + W_c + W_s \tag{1}$$

Here, W_t is the total mass loss, which is measured under corrosive slurry flow with 3.5% NaCl solution and 100 g L^{-1} sand particles. W_e is the pure erosion mass loss, which is recorded under slurry flow with 100 g L^{-1} sand particles. W_c is the pure corrosion mass loss, which is obtained under liquid flow with 3.5% NaCl solution. W_s is the mass loss from the synergism of erosion and corrosion. The mass loss rates of as-deposited Ni-Co-Fe-P coatings at impact velocity of 4.19 m s^{-1} in 3.5% NaCl solution containing 10 wt% sand particles are shown in Fig. 8. It is seen that the total mass loss W_t of Ni-Co-Fe-P coating dropped from 8.6 to 6.8 mg h^{-1} with the increasing P content and Ni-Co-Fe-12.92P coating exhibits the best erosion–corrosion resistance. Since the pure erosion mass loss W_e accounts for the largest part of W_t, as shown in Fig. 8, the erosion–corrosion resistance of Ni-Co-Fe-P coating mainly depends on its erosion resistance.

As it can be seen from Fig. 8, the pure corrosion mass loss W_c is very limited while the synergism induced mass loss W_s is obviously higher than W_c. To investigate the synergism between erosion and corrosion, the synergism rate η can be calculated as:

$$\eta = W_s/W_t \tag{2}$$

And the synergism rates η of Ni-Co-Fe-P coatings at impact velocity of 4.19 m s^{-1} are summarized in Fig. 9. As it can be seen, all of Ni-Co-Fe-P coatings exhibit positive synergy in 3.5% NaCl solution and Ni-Co-Fe-5.6P coating suffers the worst synergy. It is acknowledged that on passive metals such as stainless steel, the rate of synergy is increased by the act of solid particles damaging the surface which increases the corrosion activity hence the synergism. Since the erosion effect is similar in all of the tests in this case, the passive film is a very important factor in determining the synergism of the material. Furthermore, the erosion–corrosion rates in a stable passive film environment are higher than those in an environment where the passive film is unstable [21]. Since Ni-Co-Fe-5.6P coating possesses the most stable passive film in 3.5% NaCl solution, as shown in Fig. 6, it is possible to accelerate corrosion for the breakdown of passive film caused by particle impact. As the P content increasing from 5.6% to 12.92%, the synergy of Ni-Co-Fe-P coating continually decreased and this trend is similar with that of the total mass loss W_t. Therefore, although a material's erosion–corrosion resistance does not necessarily suffer from low synergy levels, it is very important for the total mass loss by reducing the synergy.

3.5. Worn surfaces

To assess the possible erosion–corrosion mechanism, the typical worn surfaces of Ni-Co-Fe-P coatings after 3 h erosion–corrosion at impact velocity of 4.19 m s^{-1} in 3.5% NaCl solution containing 10 wt% sand particles are shown in Fig. 10. As can be seen, heavy plastic deformation by direct particle impact is clear and corrosion is also evident due to the generation of flakes extruded from the impact scar. As shown in Fig. 10(a), cracking
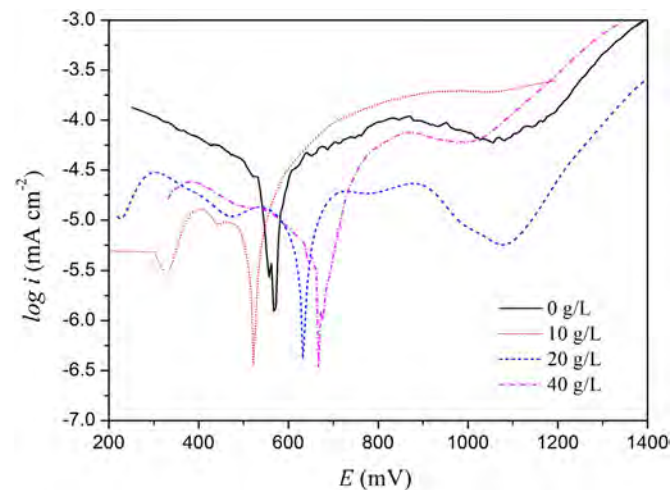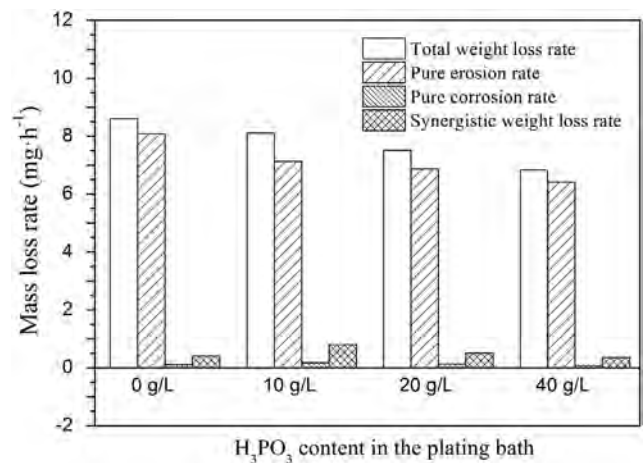

Fig. 7. Potentiodynamic polarization curves of Ni-Co-Fe-P alloy coatings in 3.5% NaCl solution with 10 wt% sand particles at impact velocity of 4.19 m s^{-1}.

Fig. 8. Relationship between mass-loss rate of Ni-Co-Fe-P coatings and H_3PO_3 concentration: (a) 0 g L^{-1}, (b) 10 g L^{-1}, (c) 20 g L^{-1} and (d) 40 g L^{-1} at impact velocity of 4.19 m s^{-1} in 3.5% NaCl slurry with 10 wt% sand particles.
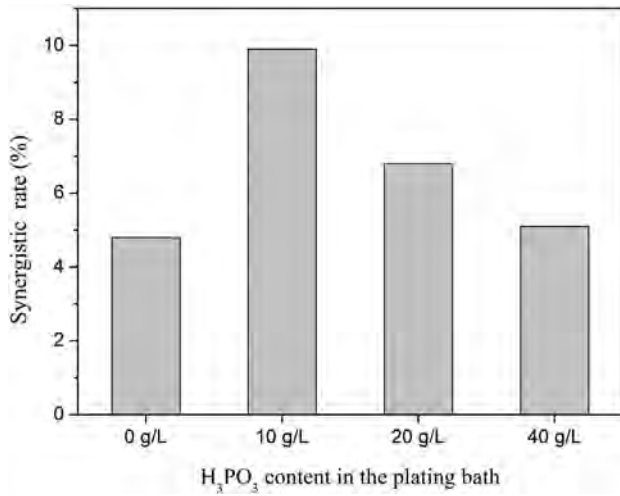
Fig. 9. Percentages of the synergistic mass loss rate for Ni-Co-Fe-P coatings.

lips along the micro-plowing grooves, and many small pitting pits can be observed on the eroded surface of Ni-Co-Fe coating. Micro-ploughing and cracking lips caused by erodent particles are also very clear on the worn surface of the as-deposited Ni-Co-Fe-P coatings, as shown in Fig. 10(b)–(d), suggesting the severe mechanical degradation is the dominant erosion–corrosion mechanism. Comparing with the Ni-Co-Fe and Ni-Co-Fe-5.6P coatings, Ni-Co-Fe-7.93P and Ni-Co-Fe-12.92P coatings were not shown any brittleness with crack characterization though their hardness was improved obviously. The worn surface of Ni-Co-Fe-12.92P coating is relatively flat with less pits and micro-cutting marks in Fig. 10(d), indicating the great corrosion resistance and highest hardness which inhibit both erosion and corrosion, and corresponding to the lowest total mass loss and synergy, as shown in Fig. 8.

4. Conclusions

Ni-Co-Fe-P quaternary alloy coatings were electrodeposited and the P content of as-deposited coating was adjusted by changing the concentration of H_3PO_3. The microstructure and erosion–corrosion resistance dependence of phosphorus content of Ni-Co-Fe-P coatings was investigated. The results showed that:

(1) The surface morphologies of the coatings exhibited colony-like structure and the increasing H_3PO_3 concentration is beneficial to grain size refinement. The phosphorus content of Ni-Co-Fe-P coating increased with the increase of H_3PO_3 concentration in the plating bath.

(2) The microstructure evolved from a composite structure of crystalline and amorphous to a pure amorphous, then to another composite structure with the increasing P content. And the microhardness of as-deposited coating increased significantly about two times.

(3) The anodic polarizations of as-deposited coatings in 3.5 wt% NaCl solution shows the corrosion resistance first decreased with the H_3PO_3 addition and then increased with more H_3PO_3 addition. A tendency to passivity can be observed from the polarization curves of as-deposited coatings and Ni-Co-Fe-12.92P coating possesses the best corrosion resistance.

(4) The mass loss rate of as-deposited coating in erosion–corrosion test indicates that high P content is beneficial to improve erosion–corrosion resistance while the synergy between erosion and corrosion is increased firstly then decreased with the increase of P content. Ni-Co-Fe-12.92P coating possesses the best erosion–corrosion resistance due to the highest hardness and the lowest corrosion current density.

(5) Mechanical micro-cutting wear mechanism prevails in these types of quaternary alloy coatings when subjected to erosion–corrosion in slurry flow.

Acknowledgment

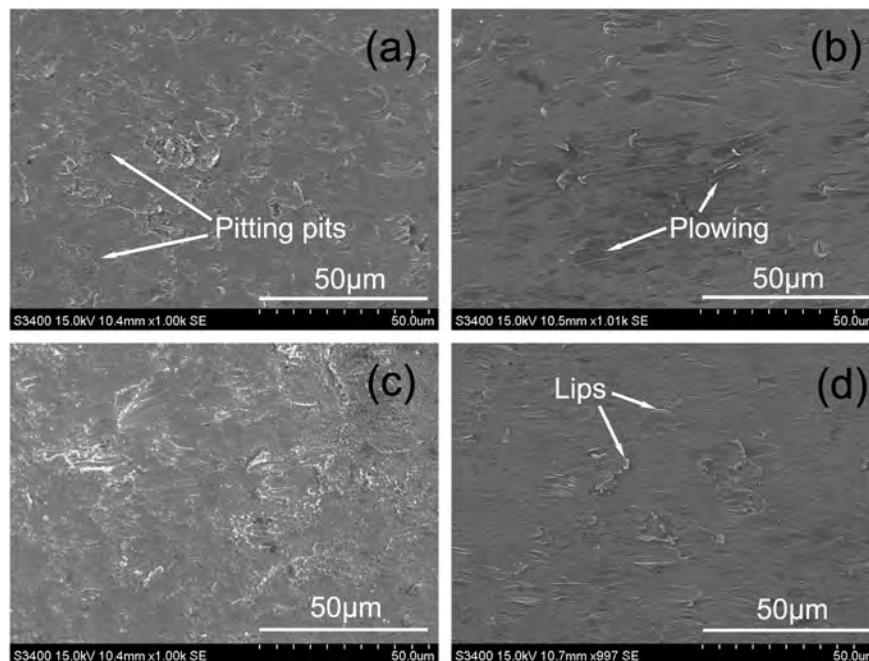**Fig. 10.** Eroded surface micrographs of Ni-Co-Fe-P coatings after erosion–corrosion tests under slurry flow at impact velocity of 4.19 m s^{-1}.

References

[1] Y. Yang, Y.F. Cheng, Electrolytic deposition of Ni-Co-SiC nano-coating for erosion-enhanced corrosion of carbon steel pipes in oilsand slurry, Surf. Coat. Technol. 205 (2011) 3198–3204.

[2] X. Ji, J. Zhao, S. Yang, L. Gu, Erosion–corrosion behavior of electrodeposited amorphous Ni-W-P coating in saline-sand slurry, Corrosion 69 (2013) 593–600.

[3] A.H. Whitehead, H. Simunkova, P. Lammel, J. Wosik, N. Zhang, B. Gollas, Rain erosion characteristics of electrodeposited Ni-SiC metal-matrix composite layers, Wear 270 (2011) 695–702.

[4] X. Ji, S. Jiang, H. Li, C. Yan, L. Jiang, Microstructure evolution and erosion–corrosion resistance of amorphous Ni-P coatings, Met. Mater. Int. 18 (2012) 655–660.

[5] M. Srivastava, V. Ezhil Selvi, V.K. William Grips, K.S. Rajam, Corrosion resistance and microstructure of electrodeposited nickel-cobalt alloy coatings, Surf. Coat. Technol. 201 (2006) 3051–3060.

[6] L. Peter, A. Csikb, K. Vadb, E. Toth-Kadar, A. Pekker, G. Molnar, On the composition depth profile of electrodeposited Fe-Co-Ni alloys, Electrochim. Acta 55 (2010) 4734–4741.

[7] Y. Yang, Preparation of Fe-Co-Ni ternary alloys with electrodeposition, Int. J. Electrochem. Sci. 10 (2015) 5164–5175.

[8] T. Osaka, Electrodeposition of highly functional thin films for magnetic recording devices of the next century, Electrochim. Acta 45 (2000) 3311–3321.

[9] X. Yuan, D. Sun, H. Yu, H. Meng, Structure and mechanical properties of Ni-P electrodeposited coatings, Appl. Surf. Sci. 255 (2009) 3613–3617.

[10] H.C. Huang, S.T. Chung, S.J. Pan, W.T. Tsai, C.S. Lin, Microstructure evolution and hardening mechanisms of Ni-P electrodeposits, Surf. Coat. Technol. 205 (2010) 2097–2103.

[11] S.Y. Kang, S.G. Yang, W.S. Hwang, Effect of phosphorous acid concentration on mechanical properties of Ni-P electrodeposits, J. Korean Inst. Chem. Eng. 48 (2015) 100–104.

[12] H.A. Ramezani-Varzaneh, S.R. Allahkaram, M. Isakhani-Zakaria, Effects of phosphorus content on corrosion behavior of trivalent chromium coatings in 3.5 wt.% NaCl solution, Surf. Coat. Technol. 244 (2014) 158–165.

[13] L.F. Lin, L.B. Lin, P.Q. Dai, Microstructure and tribological properties of electrodeposition nanocrystalline Ni-Co-Fe-P alloy coating, Tribology 31 (2011) 340–345.

[14] S.S. Rajahram, T.J. Harvey, R.J.K. Wood, Electrochemical investigation of erosion–corrosion using a slurry pot erosion tester, Tribol. Int. 44 (2011) 232–240.

[15] M.A. Farzaneh, K. Raeissi, M.A. Golozar, Effect of current density on deposition process and properties of nanocrystalline Ni-Co-W alloy coatings, J. Alloys Compd. 489 (2010) 488–492.

[16] A.M. Pillai, A. Rajendra, A.K. Sharma, Electrodeposited nickel-phosphorous (Ni-P) alloy coating: an in-depth study of its preparation, properties, and structural transitions, J. Coat. Technol. Res. 9 (2012) 785–797.

[17] J. Xu, C. Zhuo, D. Han, J. Tao, L. Liu, S. Jiang, Erosion–corrosion behavior of nano-particle-reinforced Ni matrix composite alloying layer by duplex surface treatment in aqueous slurry environment, Corros. Sci. 51 (2009) 1055–1068.

[18] M. Matsumura, Y. Oka, H. Hiura, M. Yano, The role of passivating film in preventing slurry erosion–corrosion of austenitic stainless steel, ISIJ Int. 31 (1991) 168–176.

[19] T. Hodgkiess, A. Neville, S. Shrestha, Electrochemical and mechanical interactions during erosion–corrosion of a high velocity oxy-fuel coating and a stainless steel, Wear 233-235 (1999) 623–634.

[20] Y. Zheng, Z. Yao, X. Wei, W. Ke, The synergistic effect between erosion and corrosion in acidic slurry medium, Wear 186-187 (1995) 555–561.

[21] S.S. Rajahram, T.J. Harvey, R.J.K. Wood, Erosion–corrosion resistance of engineering materials in various test conditions, Wear 267 (2009) 244–254.